Received: 27 July 2022 | Revised: 23 April 2023 | Accepted: 28 April 2023

DOI: 10.1002/mp.16521

RESEARCH ARTICLE

MEDICAL PHYSICS

# Hydrogen nanobubbles: A novel approach toward radio-sensitization agents

**Samaneh Hashemi**[1] | **Seyed Mahmoud-Reza Aghamiri**[1] | **Zahra Siavashpour**[2] | **Mahdi Kahani**[1] | **Habib Zaidi**[3] | **Ramin Jaberi**[4,5]

[1]Medical Radiation Department, Shahid Beheshti University, Tehran, Iran

[2]Radiotherapy Oncology Department, Shohada Tajrish Educational Hospital, Shahid Beheshti University of Medical Science, Tehran, Iran

[3]Geneva University Neurocenter, Geneva University, Geneva, Switzerland

[4]Cancer Institute, Tehran University of Medical Science, Tehran, Iran

[5]Medical Physics Department, Surrey University, Guildford, UK

**Correspondence**
Zahra Siavashpour, Radiotherapy Oncology Department, Shohada Tajrish Educational Hospital, Medical School, Shahid Beheshti University of Medical Science, Tehran, Iran.
Email: z_siavashpour@sbmu.ac.ir

## Abstract

**Background:** Ocular melanoma is a rare kind of eye malignancy that threatens the patient's eyesight. Radiotherapy and surgical removal are the most commonly used therapeutic modalities, and nanomedicine has lately entered this field. Brachytherapy using Ruthenium-106 ($^{106}$Ru) ophthalmic plaques has been used for decades to treat ocular melanoma, with the applicator placed on the patient's eyes until the prescribed dose reaches the tumor apex.

**Purpose:** To investigate the efficiency of hydrogen nanobubbles ($H_2$-NBs) employment during intraocular melanoma brachytherapy using a $^{106}$Ru electron emitter plaque.

**Methods:** The Monte Carlo (MC) simulation and experimental investigation using a 3D-designed phantom and thermoluminescence dosimetry (TLD) were employed. Various concentrations of $H_2$-NBs with a diameter of 100 nm were simulated inside tumor tissue. The results were presented as deposited energy and dose enhancement factor (DEF). An equivalent Resin phantom of the human eyeball was made using AutoCAD and 3D-Printer technologies. The glass-bead TLDs dosimeter were employed and placed inside the phantom.

**Results:** Using a 1% concentration of $H_2$-NBs, a DEF of 93% and 98% were achieved at the tumor apex of 10 mm from the experimental setup and MC simulation, respectively. For simulated concentrations of 0.1%, 0.3%, 0.5%, 1%, and 4% $H_2$-NBs, a maximum dose enhancement of 154%, 174%, 188%, 200%, and 300% were achieved, respectively, and a dose reduction was seen at about 3 mm from the plaque surface.

**Conclusion:** $H_2$-NBs can be used as an absorbed dose enhancer in $^{106}$Ru eye brachytherapy because of their unique physical characteristics. Reducing plaque implantation time on the patient's eye, reducing sclera absorbed dose, and decreasing the risk of patients' healthy organs irradiation are reported as some of the potential benefits of using H2-NBs.

**KEYWORDS**
brachytherapy, eye phantom, glass bead dosimeters, hydrogen nanobubbles, Ruthenium-106 ophthalmic plaque

## 1 | INTRODUCTION

Ocular melanomas can develop in four eye tissues: the uvea (UV), conjunctiva, eyelid, and eye orbit, with the uvea being the most prevalent.[1] UV melanoma (which originates in the choroid, ciliary body, or iris) is the most frequent intraocular cancer, affecting around 5 per million individuals worldwide[2] and 2500–3000 persons in North America each year.[3] Observation, surgical removal, radiation therapy, and thermotherapy (but not as a solitary initial treatment option) are the primary therapies for UV melanoma, and complete eye removal was the most prevalent treatment before the 1980s. UV melanoma radiotherapy aims to deliver a

  

sufficient radiation dose to the tumor while sparing structures near the eye or other organs at risk (OAR).[4] Brachytherapy is now the accepted standard treatment for uveal melanoma without extraocular extension, and the 1998 Collaborative Ocular Melanoma Study found no difference in survival between enucleation and globe sparing $^{125}$I brachytherapy.[5] According to comparative studies, ion therapy with radionuclides or helium ions and brachytherapy with $^{125}$I or $^{106}$Ru/$^{106}$Rh plaques give effective localized tumor management and eyesight preservation. However, proton and helium ion treatment had a greater probability of tumor recurrence than plaque treatment[6,7] Ocular brachytherapy has employed convex ophthalmic applicators, or plaques, for decades to treat malignant UV melanoma and other intraocular malignancies. Malignant melanoma, squamous carcinoma, and bulbar conjunctival cancers can be treated with a radioactive plaque of $^{90}$Sr, $^{106}$Ru, or $^{125}$I.[8] Due to the limited range of charged particles, the most appropriate radionuclides are beta-emitter $^{106}$Ru/$^{106}$Rh and $^{90}$Sr/$^{90}$Yr, which are used to treat superficial tumors. Choroidal melanomas, in particular, can be effectively treated using $^{106}$Ru applicators.[9] The beta spectrum of $^{106}$Ru radioisotope has a maximum energy of 39 keV and average energy of 10 keV. After transitioning to $^{106}$Rh and eventually to $^{106}$Pd, $^{106}$Ru becomes stable. $^{106}$Rh emits beta particles with an average and maximum energy of 1.55 MeV and 3.54 MeV, respectively.

Many studies have looked at the cytotoxicity of NPs, mostly gold, in the presence of radiation. Interest in high atomic numbers' nuclei is explained by an increase in photoelectric rate when these NPs are subjected to photon radiation. The photoelectric effect generates secondary electrons, such as photoelectrons and Auger electrons, which directly ionize DNA and destroy it. However, using nanotechnology has a different scenario in particle radiotherapy than photon beam-based radiotherapy. Hashemi et al.[10] proved that using gold NPs cannot create significant dose enhancement when they combine with beta radiation of $^{106}$Ru ophthalmic plaque. The collisional stopping power for energetic electrons diminishes with increasing atomic number.[11] Furthermore, due to the bremsstrahlung radiation, which occurs when electrons pass through a heavy nucleus, NPs with a high atomic number, such as gold, cannot be used as electron radiation-enhancing materials.[12] Electron beam energy would absorb into surrounding healthy tissues in the presence of high Z materials.

Nanobubbles (NBs) or ultrafine bubbles are gas holes with a diameter of less than one micrometer. NBs have attracted the scientific communities' interest due to their outstanding stability in recent years. This stability can last from a few weeks to a few months. Moreover, NBs have been discovered to impact the physicochemical parameters of the environment in which they are disseminated. NBs form when a homogeneous liquid changes phase due to a quick reduction in pressure below the critical point, known as cavitation. Because of their wide variety of possible applications, nanotechnology and the NBs have gotten a lot of attention in many fields, such as surfactant-free cleaning, mineral processing, intracellular drug delivery, and cancer cell drug hypersensitivity.[13] Enhanced cell membrane permeability in response to ultrasonic pulse and increased targeted intracellular drug delivery were explored by Prabhakar et al. Nanobubble-containing liposomes (NB-PTXLp) were employed for ultrasound imaging and targeted drug delivery in cancer cells in this investigation. They conclude that in MiaPaCa-2 cells, NBs and ultrasound boosted liposome absorption by 2.5 times.[14] Owen and colleagues looked at how an oral solution loaded with oxygen NBs can reduce tumor hypoxia. When compared to dissolving oxygen in water, encapsulating it in NBs delivers improved stability and concentration of oxygen based on their findings.[15] The impact of water enriched with oxygen NBs in conjunction with radiation was explored in another research study by Iijima et al., in which NBs were used to cultivate MDA-MB-231 breast cancer cells and EBC-1 lung cancer cells. Both cell samples displayed radiation resistance under hypoxic circumstances, which was considerably reduced using oxygen NBs at various radiation doses.[16]

Nanoparticles have long been explored for use in treating eye illnesses due to their ability to penetrate biological barriers that prohibit foreign compounds from entering the ocular environment. As a result, the introduction of electron radiation-sensitive nanoparticles that are compatible with the body's biological environment, specifically the eye, in this study, will open a new window for treating ocular tumors with electron plaques in a shorter time and with a more efficient dose distribution. Regarding the author's searches, there is no study on the eye's electron beam brachytherapy using nanotechnology. This study tried to address the efficacy of using $H_2$-NBs for dose enhancement during ocular brachytherapy by a $^{106}$Ru beta emitter plaque.

## 2 | METHODS

### 2.1 | Monte Carlo simulations

Simulation is a valuable and practical technique for optimizing parameters that are difficult, expensive, time-consuming, or otherwise challenging to achieve through experimentation.[10,17–19] The MCNP Monte Carlo (MC) Code for Particle and Radiation Transportation, created by the Los Alamos National Laboratory in the United States, is a well-known scientific code. This code is used as an all-purpose simulator code and as a robust tool

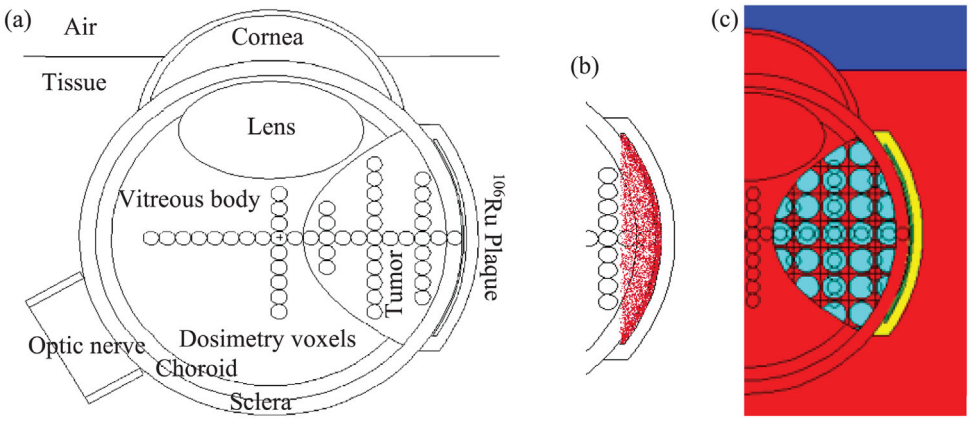


**FIGURE 1** MCNPX defined geometries of the eye, melanoma tumor, $^{106}$Ru CCA plaque, and dosimetry voxels (a); Source plot (b); and nanoparticles' distribution in tumor region (not to scale) (c).

in particle and ionizing ray transport, such as protons, neutrons, electrons, and photons.[20,21] The MCNPX code was employed as one of the most extensively used and powerful versions in this research. Because of the nature of particle transport, the statistical uncertainty of the MCNPX simulation results diminishes with the increasing number of runs. The number of particles in each program in this investigation was chosen so that the statistical error in all performances was less than 5%.

### 2.1.1 | Eyeball and plaque simulation

Human eye geometry was considered to mimic the entire eyeball, including the sclera, choroid, lens, cornea, optic nerve, and tumor by MCNPX; previous research was employed.[22,23] Simulated geometries can be seen in Figure 1. All the simulated phantoms were filled with water in the first stage. The dosimetry was carried out using tally * F8 and spheres having a radius of 0.5 mm along the plaque's central axis and in the form of profiles created at various depths. Distinct elements of the eye, such as sclera, lens, or etc. were designated as a cell, and energy deposition in each was computed. The tumor was networked depending on the concentration and size of NBs, and the investigated NBs were defined inside it using the "lattice" command and "fill" card.[24] It was networked in three dimensions by lattice definition and then a spherical with radius of 100 nm was defined inside of each voxel by "fill" instruction, which represents a nanobubble. The network uses the same material as the tumor, but the spherical is filled with Hydrogen gas. Using Zhang's research[25] as a reference, the network size was determined based on the concentration of related nanoparticles.

Two concentric spheres intersected by a cylinder were used to represent the geometry of CCA model $^{106}$Ru eye plaque (Bebig, Eckert & Ziegler, Germany) in the code. The diameter of the cylinder was 15.3 mm, and the radial difference between the two circles was 1 mm (equal to the plaque thickness). The $^{106}$Ru radioactive cell was also defined using the same shape. Plaque cells with three layers of 0.1, 0.2, and 0.7 mm were delineated on the sclera and tumor with a height of 10 mm above the sclera surface (Figure 1).

### 2.1.2 | Hydrogen nanobubbles simulation

*Hydrogen nanobubbles*

In radiation dosimetry, having precise information on the energy loss of charged particles in various materials is critical and stopping power is the most crucial quantity utilized for charged particles. The average energy dissipated by ionizing radiation in a medium per unit length of the radiation route in that medium is described by ICRU* as stopping power. Bethe (1933 and 1953) formulated the calculation of the stopping power due to the colonic interactions of charged particles by taking into account the particle's charge, mass, and velocity (energy), as well as the density and the atomic number of the adsorbent.[26] The quantity of electron energy absorption in a medium is proportional to the ratio of atomic number (Z) to the medium material's mass number (A), as shown by the collisional stopping power formula. Figure 2 depicts an electron's stopping power with energies of 1, 2, and 3 MeV, as calculated by the report.[26] Because the electron energy released by a $^{106}$Ru nucleus lies in this range, these three energies were chosen. The clear distinction between hydrogen and other elements stands out in this figure.

Therefore, the hypothesis of the current study, which was the use of hydrogen gas as a dose enhancer and

* International Commission on Radiation Units & Measurements

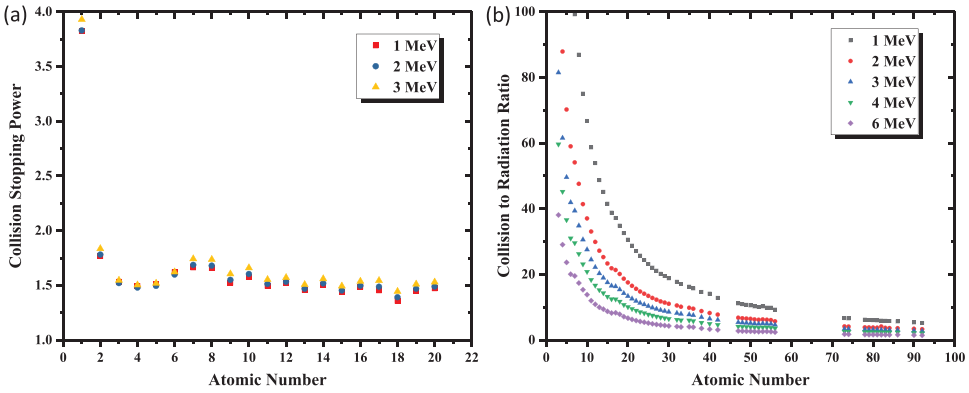


**FIGURE 2** (a) Collisional stopping power versus atomic number for three different electron energies; (b) The ratio of collisional to radiation stopping power for different electron energies. (Data were derived from Pages et al.[26]).

in the form of NBs, was examined. Five concentrations of $H_2$-NBs were specified inside the tumor to investigate their influence on the tumor's absorbed dose at different depths. Hydrogen is a colorless, odorless, and non-toxic gas in general. However, it is very flammable and highly explosive when mixed with air at a concentration of 4%–74%.[27] As a result, in the experiments conducted in this study, the maximum hydrogen concentration evaluated was 4%. Five hydrogen concentrations of 0.1%, 0.3%, 0.5%, 1%, and 4% by volume were addressed during the simulations. The NBs were defined to have a diameter of 100 nm. In addition to the dosimetry calculated by the tally *F8, the electron energy flux at different depths of the plaque surface was also measured before and after adding $H_2$-NB using the tally F4 of the MCNPX code.

### 2.1.3 | Glass beads and phantom simulation

Glass beads contain thermoluminescence (TL) capabilities, according to studies done in 2008 and 2012.[28,29] However, Jafari et al. researched these beads as radiation dosimeters and investigated their characteristics in detailed studies.[30,31] The glass beads were found to have a good spatial resolution (1–3 $mm^3$), cheap cost, reusability, and strong ineffectual nature. They are less faded by radiation exposure, have high TL light transparency, high sensitivity, and a huge dynamic dose range that stays linear from 1 cGy to 100 Gy compared to commercial TLD LiF dosimeters. They have also been found to be unaffected by radiation doses and angle of impact and have modest response variations in the MeV range for electron and photon beams. The density of these glass beads is measured as $2.09 \pm 0.01$ $g/cm^3$, and the composition of their elements was listed in the previous study by Jafari et al.[30] The cylindrical glass beads utilized in this study had an inner radius of 0.3 mm, an outer radius of 0.75 mm, and a height of 1.2 mm. The MCNPX code was used to model these dosimeters with their exact parameters, and the phantom geometry was developed to be compatible with experimental data to improve accuracy. Therefore, the phantom material was considered resin in this simulation, like the experimental one.

## 2.2 | Experimental dosimetry

### 2.2.1 | Phantom and TLDs

The experimental eye phantom was constructed to match the actual size of the eye so that the ocular plaque may be readily put on it, as well as to retain a solution containing $H_2$-NBs inside the tumor volume. As a result, the phantom was created in 3D using AutoCAD software. The tumor chamber was hollowly inserted in the phantom, 10 mm above the surface of the eyeball, to accommodate $H_2$-NBs. In addition, three distinct compartments for glass beads were put so that a dosimeter could be placed behind the tumor. Figure 3a,b illustrate the AutoCAD-designed phantom and the constructed phantom holder for the stable placing of brachytherapy plaques.

Inside the tumor volume, seven glass beads with a height of 1.2 mm were vertically stacked in a row through the plaque's central axis. Similarly, three strands of glass beads were placed in three cylindrical holes at the back of the pseudotumor cell. With these dosimeter arrangements, dosimetry could be carried out horizontally and perpendicular to the plaque's central axis. A PTW FIMEL LTM equipment was utilized to take TLD readings at a TLD lab. The reading parameters were chosen following the methodology recommended by the manufacturer of these TLDs. TLD calibration was carried out by a 6 MeV electron beam of a linear accelerator with the maximum, minimum, and average uncertainty of 9.5%, 0.4%, and 2.8%, respectively.

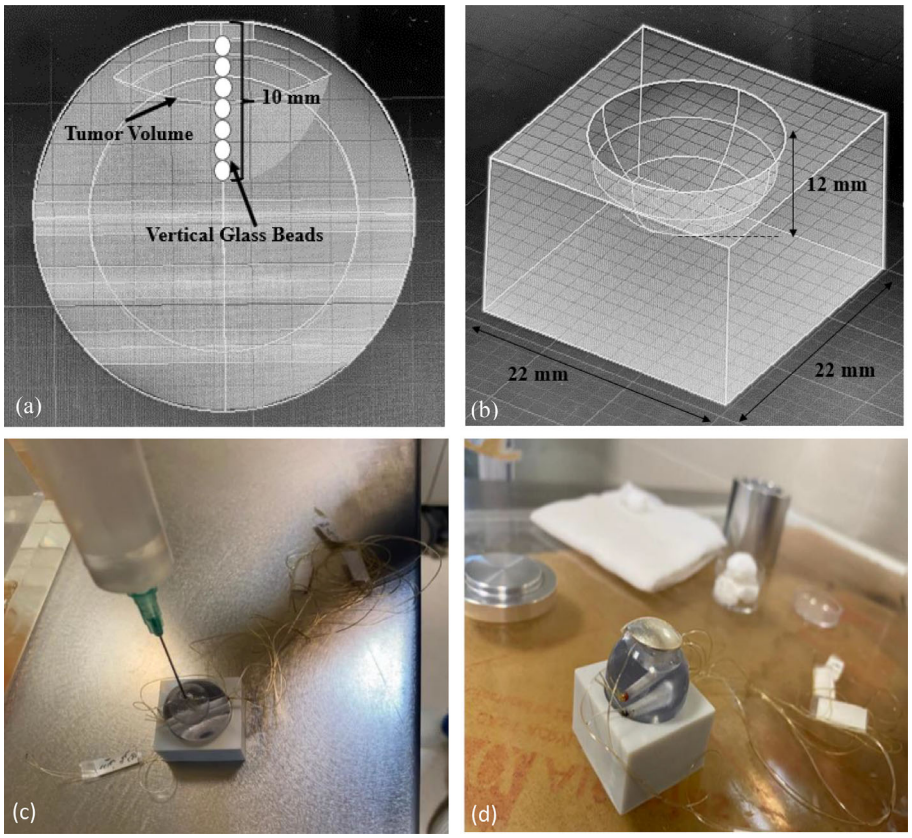


**FIGURE 3** (a) Eye phantom designing by 3D AutoCAD, and a schematic view of placing vertical glass beads, and (b) a phantom container, (c) injection of fluid into the tumor region implanted within the phantom; in the first step, water, and in the second stage, hydrogen-enriched water was used. (d) placing a CCA over the phantom inside a hospital.

### 2.2.2 | H2-NBs and experimental setup

One of the most crucial challenges of the current study was preparing $H_2$-NBs solutions. Generally, air and oxygen NBs are created inside the water fluid, which is employed for water purification or materials science (such as concrete production).[32,33] Following up on this NB manufacturing, a Nanotechnology Company could make it in water fluid with a concentration of 1%.

A Bebig CCA model of $^{106}$Ru ophthalmic plaque was implanted on a phantom at Torfeh educational hospital, Tehran, Iran. For 6 h, the plaque was placed over the phantom. The first stage involved filling the tumor volume with water and repeating the procedure two times. Figure 3c,d depicts the injection of fluid into this location. The tumor volume was filled with hydrogen-enriched water in the second step. The findings were compared to the initial data and presented as a dose curve and a dose enhancement factor (DEF). DEF was calculated using formula.[1]

$$\text{Dose Enhancement Factor (DEF)}\,\% = \left(\frac{\text{Dose}\ (\text{Water} + H_2 - \text{NBs})}{\text{Dose}\ (\text{Water})} - 1\right) \times 100 \quad (1)$$

## 3 | RESULTS

### 3.1 | Simulation validation

The simulation results for glass beads and the resin phantom are shown in Figure 4 and compared to experimental data. The maximum, minimum, and average relative differences for these two sets of data are reported as 14%, 0%, and 1.6%, respectively.

### 3.2 | Dose enhancement factor

#### 3.2.1 | 1% H2-NBs and resin phantoms

Figure 5 shows the outcome of simulation (a) and experiments (b) in terms of energy deposition, dose, and DEFs. As shown in this image, adding $H_2$-NBs at the concentration of 1% raises DEF by 98% and 94% toward the tumor's apex in the simulation and experiments, respectively. These values have also been determined to be negative at the tumor base, −12% at 1.5 mm from the plaque in simulation and −2.8% at the first point of experimental dosimetry (≈ 2 mm). However,

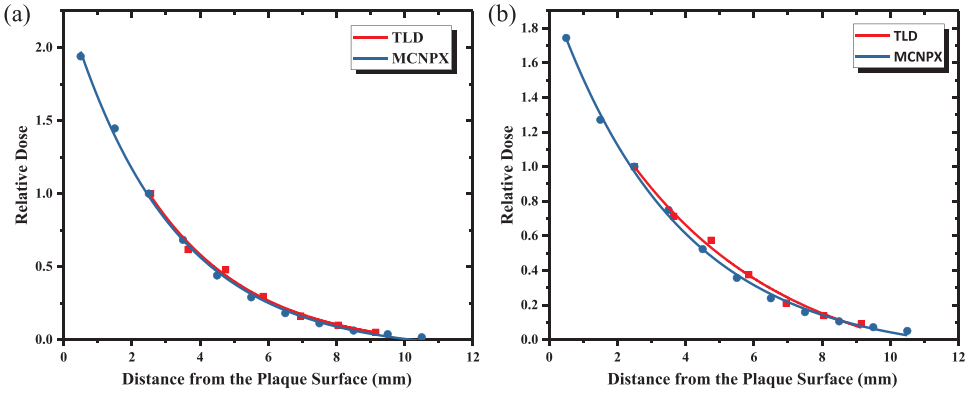


**FIGURE 4** Water- (a) and water + 1% hydrogen NBs (b) filled tumor in a phantom: Comparison of simulated and experimental results.

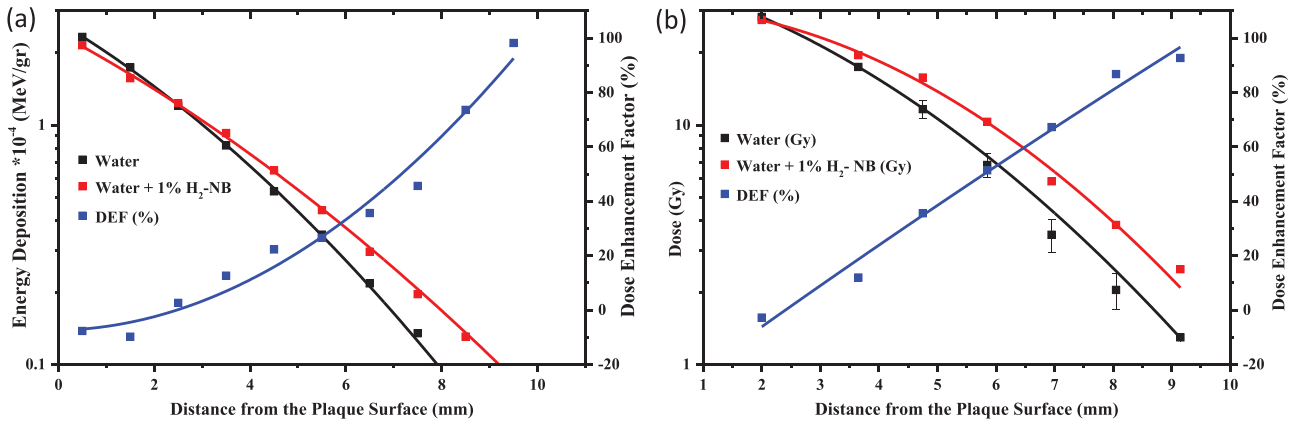


**FIGURE 5** Simulation (a) and experimental (b) results as well as DEF after adding 1% $H_2$-NB inside the tumor volume.

**TABLE 1** Experimental results for glass beads located inside the tumor volume along the central axis of the plaque.

| | Raw data | | Dose (Gy) | | |
|---|---|---|---|---|---|
| TLD no. | Water | Water + 1% $H_2$-NBs | Water ($D_1$) | Water + 1% $H_2$-NB ($D_2$) | $D_2/D_1$ |
| 1 | 132 178.7 ± 909.13 | 12 8525.8 | 28.261 ± 0.194 | 27.479 | 0.972 |
| 2 | 81 845.47 ± 376.5 | 91 594.47 | 17.486 ± 0.080 | 19.573 | 1.119 |
| 3 | 54 555.74 ± 4347.37 | 73 904.26 | 11.644 ± 0.928 | 15.786 | 1.356 |
| 4 | 31 984.02 ± 3358.3 | 48 324.22 | 6.812 ± 0.715 | 10.310 | 1.514 |
| 5 | 16 414.57 ± 2215.56 | 27 365.41 | 3.479 ± 0.470 | 5.819 | 1.673 |
| 6 | 9729.942 ± 1442.4 | 18 026.17 | 2.048 ± 0.304 | 3.824 | 1.867 |
| 7 | 6226.467 ± 136.36 | 11 906.77 | 1.298 ± 0.028 | 2.514 | 1.937 |

the DEF becomes higher by getting closer to the tumor apex, which is more tangible in the exact amounts of data extracted from the vertical strand of glass beads located inside the fabricated phantom that are given in Table 1.

### 3.2.2 | Different concentrations of H2-NB in the water phantom

Five different concentrations of $H_2$-NB with a diameter of 100 nm were simulated at 0.1%, 0.3%, 0.5%, 1%, and

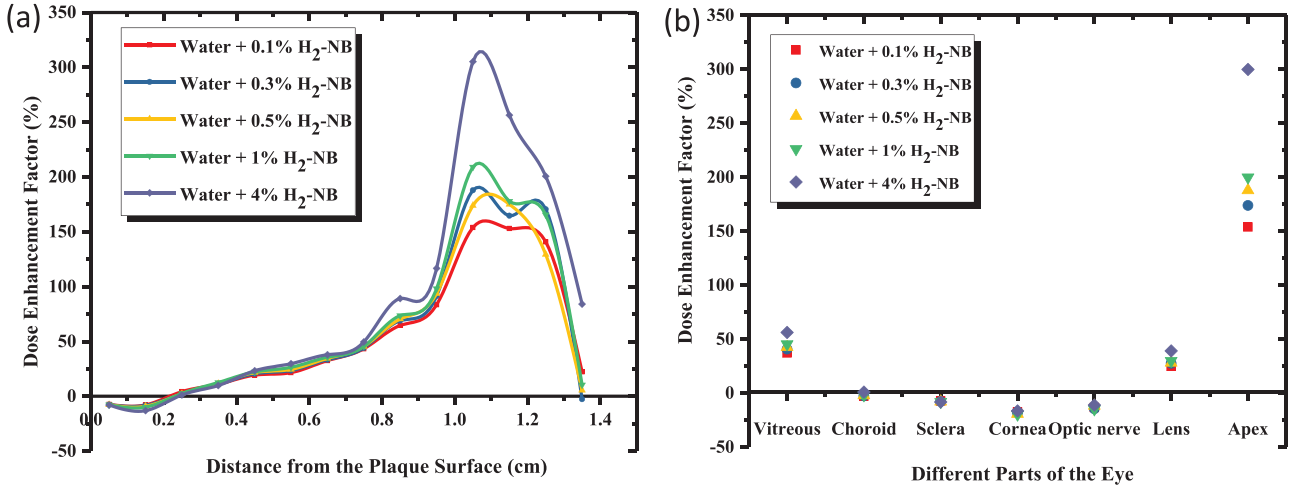


**FIGURE 6** (a) DEFs for hydrogen along the direction of the plaque's central axis compared to the distance from the plaque at five simulated concentrations and a diameter of 100 nm. (b) DEFs for different parts of the eye based on simulation results.

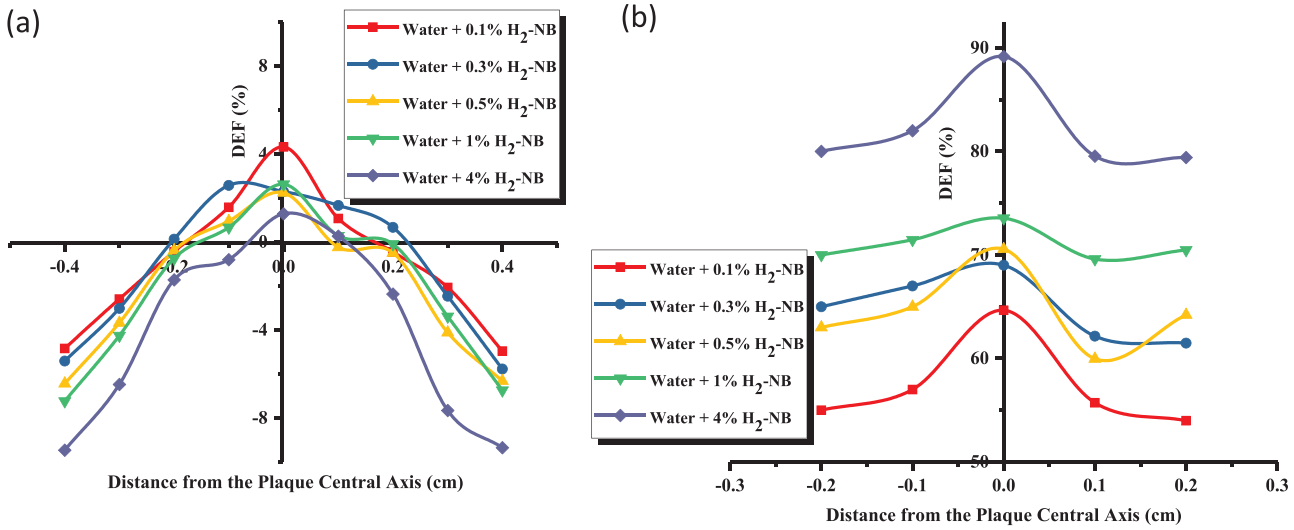


**FIGURE 7** DEFs for hydrogen at 2.5 mm (a) and 8.5 mm (b) from the plaque surface versus depth at five simulated concentrations and 100 nm diameter.

4% by volume inside the tumor. Figure 6a depicts the DEFs for various concentrations of $H_2$-NBs along the plaque's central axis. As it can be seen in this graph, the difference in hydrogen concentrations becomes more significant as you move farther away from the plaque. Thus, with a concentration of 4%, an increased dose of 300% is reported at the tumor's apex (11 mm). On the contrary, the first 3 mm interval dedicates itself to a dose reduction that could significantly reduce the absorbed dose of the sclera, as can be seen in Figure 6b. The dose profiles obtained at 2.5 and 8.5 mm from the plaque surface are presented in Figure 7. As can be observed, the rate of dose augmentation rises with distance from the plaque for various hydrogen concentrations. Changes in the production of electron intensity in the tumor volume after adding $H_2$-NB by the concentration of 4% (the maximum permitted concentration) were obtained, as illustrated in Figure 8.

## 4 | DISCUSSION

This study aimed to find and introduce a method for using nanotechnology in eye brachytherapy with electron particles. A protocol that intends to increase the absorption dose of electron-emitting $^{106}$Ru ophthalmic plaques in the treatment of ocular melanoma was presented. Based on Figure 2 no material can operate like hydrogen to stop energetic electrons using collisional

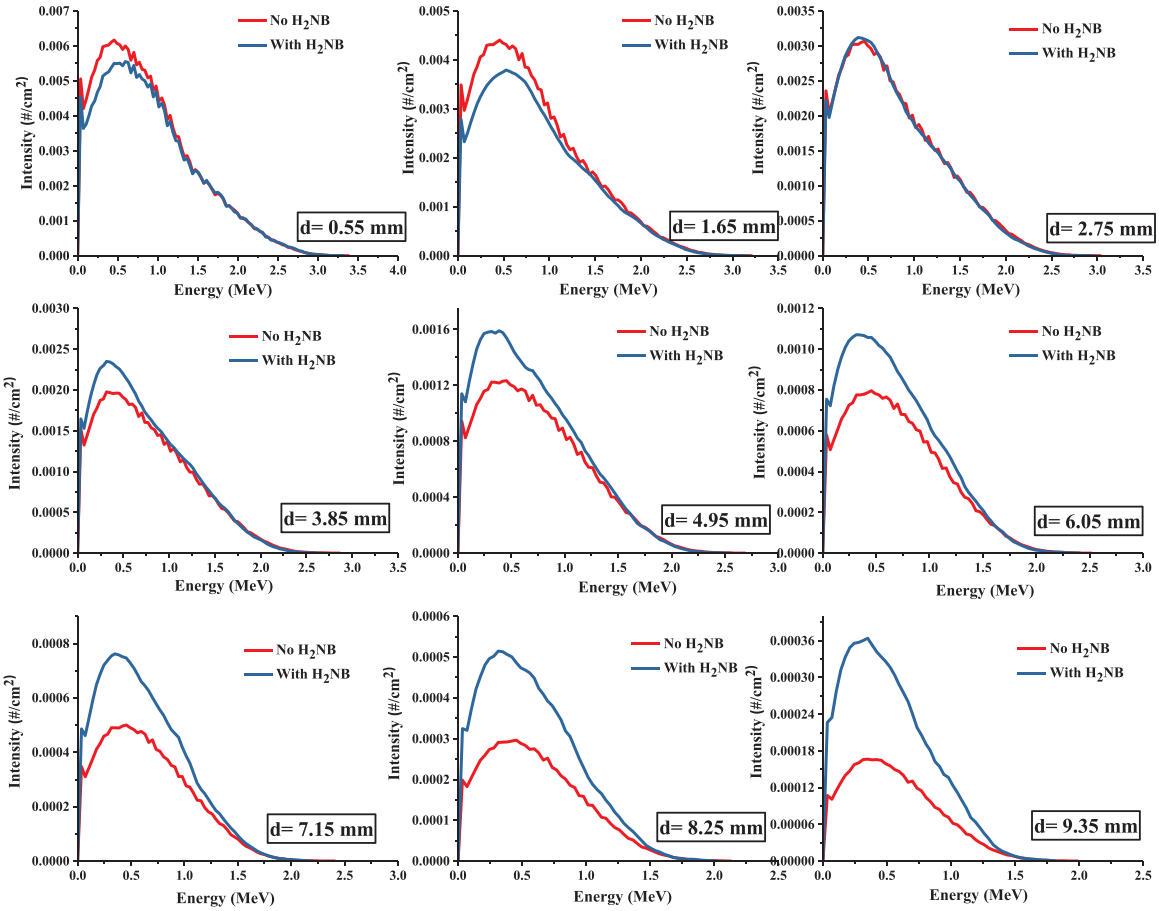


**FIGURE 8** Energy flux of electron intensity in the tumor volume with and without 4% $H_2$-NBs; d, depth of measurement.

and radiation-stopping power characteristics for electrons in the mega-electron-volt energy range. Hydrogen has the power to halt more than double the impact of all matter against electrons due to its high electron density, which is nearly double that of all succeeding elements. The hydrogen nucleus is the unique element with a Z/A ratio of one since it only has one proton, which is about 0.5 for the other elements. The ratio of collisional to radiation stopping power for an electron at five different energies is also shown in Figure 2b. This graph is essential because bremsstrahlung radiation should be addressed when selecting an electron absorber since materials with a high atomic number emit some of the electron energy as photon radiation. The superiority of hydrogen over other elements is evident in this graph. Generally, Hydrogen is one of the most promising gases, and it has been at the forefront of studies, including in medicine. No biotoxicity has been reported for hydrogen gas in studies, and the maximum permitted concentration of 4% was used in this study because of flammability considerations.

Figure 4 represents the simulation validation results with experimental measurements. The closeness of these two curves shows that the simulation was able to precisely see the planned configuration and CCA plaque and compute the correct results. Inside the tumor, water enriched with 1% $H_2$-NBs was described as circular NBs with a diameter of 100 nm. The initial measurement point was taken at this location since the first glass bead distance was 2 mm from the plaque's surface, and the simulation and experimental findings were then normalized at this dose. This measured data in the form of energy deposition, dose, and DEFs has been shown in Figure 5. Introducing $H_2$-NBs at the concentration of 1% raises DEF by 98% and 94% at the tumor's apex with a negative amount of −12% (at 1.5 mm) and −2.8% (≈ 2 mm) at the base in the simulation and experiments, respectively. These results may help to improve the quality of $^{106}$Ru ocular plaque therapy. Because the dose delivered to the tumor's apex is always the criterion in treatment planning with these plaques, the plaque is implanted on the patient's eye until the specified dose is delivered to the tumor's apex. As a result, the tissues will be exposed to greater doses at shorter distances, resulting in non-homogeneous dose distribution. The findings suggest that using $H_2$-NBs enhances the dose in tumor tissue while also helping to homogenize the dose distribution.

Similar trends were seen in Figure 6a where five different concentrations of $H_2$-NB introduced inside the tumor in the Monte Carlo space. This figure shows that using different $H_2$-NB concentrations has no significant discrepancies as dose enhancers in the early interval's plaque surface. However, DEF differences become wider at 0.8–1.2 cm intervals facing the active plaque surface, and there are peaks for all concentrations at about 1.1 cm. For concentrations of 0.1%, 0.3%, 0.5%, and 1%, DEF is 154%, 174%, 188%, and 200%, respectively. Two dose profiles inside the tumor volume at 2.5 and 8.5 mm from the plaque surface are shown in Figure 7. The $^{106}$Ru plaque (without NBs) exhibits a dramatic dose drop with increasing distance from the plaque due to beta particle radiation, which causes the deeper tissues to receive a substantially lower proportion of the plaque's radiation exposure. According to Figure 7b, the inclusion of 4% $H_2$-NPs has been shown to double the dose at a distance of 8.5 mm from the plaque, making the usage of these plaques more effective in deeper tumors. It is also worth noting that the profiles have a peak in the direction of the plaque axis at both distances. Because of the plaque's convex form and the existence of more $H_2$-NPs in this direction than in the corners, more interactions may be expected, resulting in increased electron absorption in this path. Another obvious point in Figure 7a is significant negative amounts of DEFs that directly depend on NBs' concentration. This amount reaches −10% in the case of 4% concentration. Head-on collisions of ruthenium beta particles with an electron cloud because of the hydrogen presence, resulting in the generation of higher energetic secondary electrons, extending the range of these electrons. Thus, the electrons are absorbed, and their energy is deposited at a greater distance than usual, around 3 mm. Figure 8 depicts a better view of understanding what happened in the tumor region by introducing $H_2$-NB resulting from a collision between $^{106}$Ru emitted electrons and the medium materials. The distance of 2.7 mm from the plaque surface is a watershed in this graph. In the water-only medium, more electrons were created at closer distances, whereas the introduction of hydrogen reduced their creation. But after this point, electron production increased gradually and reached its maximum number at the tumor apex.

In a nutshell, three points of view can be brought forward to explain the dose changing mechanism in $^{106}$Ru brachytherapy in the presence of $H_2$-NBs:

1. The range-energy approach for beta particles emitted by $^{106}$Ru source:

   Considering the energy spectrum of $^{106}$Ru radioisotope, it has a beta energy of 1.3 MeV on average and maximum energy of 3.5 MeV. These energies will result in electron ranges of 0.5 cm and 1.7 cm in water medium, respectively.[34] Therefore, $^{106}$Ru high-energic beta radiation can escape from a target with 1 cm depth. A hydrogen atom's electron density permits to create a concentrated electrical cloud inside the medium. As a result, if released into the environment, it will act as a beta ray trap, lowering the electron's range. This helps to explain why the tumor apex has a high DEF. Figure 6b depicts the distinct variation in DEF between the apex and the rest of the eye.
2. Gaseous approach of introducing $H_2$-NBs into a target:

   The addition of hydrogen gas into the tumor volume in the form of NBs allows $^{106}$Ru's beta particles to travel more freely in the target volume. Due to its gaseous nature, hydrogen has a far lower density than water, allowing beta particles to penetrate deeper in the hydrogen environment than in the water environment. For this reason, Figure 8 and the drop in electron flow in the first 3 mm may be explained.
3. Repulsive energy approach between hydrogen electronic clouds and $^{106}$Ru beta particles:

   When we go back to basic physics and the way that particles interact, we recall that particles with the same charge repel each other. Because of the repulsive effect, $^{106}$Ru's beta particles in a negatively charged environment (due to the presence of hydrogen) can traverse a longer distance than in the normal state. This becomes much more tangible when we see the electron as a wave rather than a particle.

According to the results of this study, the following might be some of the benefits of employing $H_2$-NBs in the treatment of ocular melanoma and the use of brachytherapy for $^{106}$Ru plaque based on the physical parameters investigated in this study:

1. At the tumor's apex, a 2-fold increase in dose at 1% hydrogen concentration (obtained in both simulation and experimental studies) and a 4-fold increase in 4% concentration (simulation) could cut the treatment time by 50% and 25%, respectively. As a result, the use of $H_2$-NBs greatly decreases treatment duration, which can be up to 250 h in some situations and the patient's stay in the hospital.
2. More patients (about four times) will be treated with one plaque.
3. The financial burden placed on the patient and the hospital is lessened.
4. The risk of unintended irradiation of vital organs near the tumor will be decreased, allowing the radiation therapy aims to be effectively pursued (the ratio of tumor dose to healthy surrounding tissue will increase).

However, clinical studies should confirm these potential benefits. The level of $H_2$-NB absorption in healthy tissues surrounding ocular melanoma and its impact on

their absorbed dose are additional difficulties that need to be covered in future investigations. More accurate outcomes will be obtained by addressing this issue in laboratory research and in vivo animal studies.

## 5 | CONCLUSION

For the first time, $H_2$-NBs were employed as electron radiation-sensitive materials in ocular melanoma brachytherapy in this work. Hydrogen has been utilized as a therapeutic gas in medical investigations, but this effort is the first to use it in the form of NBs in conjunction with electron beam therapy. According to this study, the presence of $H_2$-NBs in melanoma tumor tissue can enhance the dose by up to 300%, greatly reducing the duration of the plaque on the human eye. A dedicated phantom was designed and constructed that can be employed with different host materials as a tumor and nanoparticles/bubbles as dose enhancers during ophthalmic studies as well as $^{106}$Ru ocular plaques commissioning and quality control. Glass bead TLDs were also used, which are relatively new and robust dosimeters in small radiation fields with high dose gradients.

### ACKNOWLEDGMENTS

This research received no specific grant from any funding agency in the public, commercial, or not-for profit sectors.

### CONFLICT OF INTEREST STATEMENT

The authors have no relevant conflicts of interest to disclose.

### REFERENCES

1. Shields J, Shields C, Chandra SR. Intraocular tumors: a text and atlas. *Arch Ophthalmol-Chicago*. 1994;112(2):169.
2. Singh AD, Turell ME, Topham AK. Uveal melanoma: trends in incidence, treatment, and survival. *Ophthalmology*. 2011;118(9):1881–1885.
3. Shields CL, Shields JA. Ocular melanoma: relatively rare but requiring respect. *Clin Dermatol*. 2009;27(1):122–133.
4. Nag S, Quivey JM, Earle JD, et al. The American Brachytherapy Society recommendations for brachytherapy of uveal melanomas. *Int J Radiat Oncol Biol Phys*. 2003;56(2):544–555.
5. Joh S, Kim ME, Reilly M, et al. Outpatient ocular brachytherapy: the USC experience. *Adv Radiat Oncol*. 2021;6(5):100737.
6. Hungerford J, Foss A, Whelahan I, Errington R, Kacperek A, Kongerud J. Side effects of photon and proton radiotherapy for ocular melanoma. *Radiotherapy of Ocular Diseases*. Karger Publishers; 1997:287–293. 30.
7. Wilson MW, Hungerford JL. Comparison of episcleral plaque and proton beam radiation therapy for the treatment of choroidal melanoma. *Ophthalmology*. 1999;106(8):1579–1587.
8. Stannard C, Sauerwein W, Maree G, Lecuona K. Radiotherapy for ocular tumours. *Eye*. 2013;27(2):119–127.
9. Mowlavi AA, Yazdani M. Monte Carlo simulation of two 106Ru eye plaques in a new mathematical human eye model. *Iran J Nucl Med*. 2008;16(2):16–22.
10. Hashemi S, Aghamiri M, Kahani M, Jaberi R. Investigation of gold nanoparticle effects in brachytherapy by an electron emitter ophthalmic plaque. *Int J Nanomed*. 2019;14:4157–4165.
11. Berger MJ, Coursey JS, Zucker MA, Chang J, Stopping-power and range tables for electrons, protons, and helium ions, NIST Standard Reference Database 124. National Institute of Standards and Technology. 2017. https://dx.doi.org/10.18434/T4NC7P
12. Litovchenko VY, Vasutin NA, Tashlykov OL, Kozlov AV, Seleznev EN, Modeling radiation protection of containers for transporting isotopes with high-energy beta irradiation. InAIP Conference Proceedings 2019;2174(1):020134. AIP Publishing LLC
13. Michailidi ED, Bomis G, Varoutoglou A, Efthimiadou EK, Mitropoulos AC, Favvas EP. Fundamentals and applications of nanobubbles. *Interface Science and Technology*. Elsevier; 2019:69–99. 30.
14. Prabhakar A, Banerjee R. Nanobubble liposome complexes for diagnostic imaging and ultrasound-triggered drug delivery in cancers: a theranostic approach. *ACS Omega*. 2019;4(13):15567–15580.
15. Owen J, McEwan C, Nesbitt H, et al. Reducing tumour hypoxia via oral administration of oxygen nanobubbles. *PLoS One*. 2016;11(12):e0168088.
16. Iijima M, Gombodorj N, Tachibana Y, et al. Development of single nanometer-sized ultrafine oxygen bubbles to overcome the hypoxia-induced resistance to radiation therapy via the suppression of hypoxia-inducible factor-1$\alpha$. *Int J Oncol*. 2018;52(3):679–686.
17. Kahani M, Mahdi M, KamaliAsl A, Hashemi S, Ghadiri H. Simultaneous use of two different contrast agents and assessing their accuracy in breast tissue using dual-energy digital mammography. *J Maz Univ Med*. 2015;24(122):239–251.
18. Kahani M, Kamali-asl A, Ghadiri H, Hashemi S. A method for material decomposition in dual-energy contrast enhancement digital mammography. *Measurement*. 2016;88:87–95.
19. Kamrani S, Aghamiri SMR, Hashemi S. Dose characteristics of Au-198 eye brachytherapy applicator: a Monte Carlo study. *Appl Radiat Isot*. 2021;176:109866.
20. Hendricks JS, McKinney GW, Fensin ML, et al. *MCNPX 2.6. 0 Extensions*. Los Alamos National Laboratory; 2008.
21. Kahani M, Kamali-Asl A, Tabrizi SH. Proposition of a practical protocol for obtaining a valid radiology image using radiography tally of MCNPX Monte Carlo code. *Appl Radiat Isot*. 2019;149:114–122.
22. Yoriyaz H, Sanchez A, Dos Santos A. A new human eye model for ophthalmic brachytherapy dosimetry. *Radiat Prot Dosim*. 2005;115(1-4):316–319.
23. Asadi S, Vaez-zadeh M, Masoudi SF, Rahmani F, Knaup C, Meigooni AS. Gold nanoparticle-based brachytherapy enhancement in choroidal melanoma using a full Monte Carlo model of the human eye. *J Appl Clin Med Phys*. 2015;16(5):344-357.
24. Hashemi S, Aghamiri SMR, Jaberi R, Siavashpour Z. An in silico study on the effect of host tissue at brachytherapy dose enhancement by gold nanoparticles. *Brachytherapy*. 2021;20(2):420–425.
25. Zhang SX, Gao J, Buchholz TA, et al. Quantifying tumor-selective radiation dose enhancements using gold nanoparticles: a Monte Carlo simulation study. *Biomed Microdev*. 2009;11:925.
26. Pages L, Bertel E, Joffre H, Sklavenitis L. Energy loss, range, and bremsstrahlung yield for 10-keV to 100-MeV electrons in various elements and chemical compounds. *At Data Nucl Data Tables*. 1972;4:1–27.
27. Li S, Liao R, Sheng X, et al. Hydrogen gas in cancer treatment. *Front Oncol*. 2019;9:696.

28. Moffatt J, Spooner N, Creighton D, Smith B. Luminescence properties of common glasses for application to retrospective dosimetry. *Radiat Meas*. 2012;47(9):851–856.
29. Zacharias N, Beltsios K, Oikonomou A, et al. Solid-state luminescence for the optical examination of archaeological glass beads. *Opt Mater*. 2008;30(7):1127–1133.
30. Jafari S, Jordan T, Hussein M, et al. Energy response of glass bead TLDs irradiated with radiation therapy beams. *Radiat Phys Chem*. 2014;104:208–211.
31. Jafari S, Bradley D, Gouldstone C, et al. Low-cost commercial glass beads as dosimeters in radiotherapy. *Radiat Phys Chem*. 2014;97:95–101.
32. Pourkarimi Z, Rezai B, Noaparast N. Effective parameters on generation of nanobubbles by cavitation method for froth flotation applications. *Physicochem Probl Miner Process*. 2017;53(2):920–942.
33. Arefi A, Saghravani SF, Mozaffari Naeeni R. Mechanical behavior of concrete, made with micro-nano air bubbles. *Civ Eng Infrastruct J*. 2016;49(1):139–147.
34. Cember H, Johnson TE, Alaei P. Introduction to health physics. *Med Phys*. 2008;35(12):5959.

**How to cite this article:** Hashemi S, Aghamiri SM-R, Siavashpour Z, Kahani M, Zaidi H, Jaberi R. Hydrogen nanobubbles: A novel approach toward radio-sensitization agents. *Med Phys*. 2023;50:6589–6599.
https://doi.org/10.1002/mp.16521